

Simultaneous estimation of aerosol optical constants and size distribution from angular light-scattering measurement signals

Zhen-Zong He(贺振宗), Dong Liang(梁栋), Jun-Kui Mao(毛军逵), Xing-Si Han(韩省思)
Citation: Chin. Phys. B . 2018, 27(5): 059101. **doi:** 10.1088/1674-1056/27/5/059101

Journal homepage: http://cpb.iphy.ac.cn; http://iopscience.iop.org/cpb

What follows is a list of articles you may be interested in

Thermal conductivity of carbon nanotube superlattices: Comparative study with defective carbon nanotubes

Kui-Kui Zhou(周魁葵), Ning Xu(徐 宁), Guo-Feng Xie(谢国锋)
Chin. Phys. B . 2018, 27(2): 026501. **doi:** 10.1088/1674-1056/27/2/026501

Thermal conductivity of carbon nanoring linked graphene sheets:A molecular dynamics investigation

Gang Shi(石刚), Jianwei Zhang(张鉴炜), Yonglv He(贺雍律), Su Ju(鞠苏), Dazhi Jiang(江大志)
Chin. Phys. B . 2017, 26(10): 106502. **doi:** 10.1088/1674-1056/26/10/106502

Influence of surface scattering on the thermal properties of spatially confined GaN nanofilm

Yang Hou(侯阳), Lin-Li Zhu(朱林利)
Chin. Phys. B . 2016, 25(8): 086502. **doi:** 10.1088/1674-1056/25/8/086502

Thermodynamic behaviour of Rashba quantum dot in the presence of magnetic field

Sukirti Gumber, Manoj Kumar, Pradip Kumar Jha, Man Mohan
Chin. Phys. B . 2016, 25(5): 056502. **doi:** 10.1088/1674-1056/25/5/056502

Effects of in-plane stiffness and charge transfer on thermal expansion of monolayer transition metal dichalcogenide

Wang Zhan-Yu, Zhou Yan-Li, Wang Xue-Qing, Wang Fei, Sun Qiang, Guo Zheng-Xiao, Jia Yu
Chin. Phys. B . 2015, 24(2): 026501. **doi:** 10.1088/1674-1056/24/2/026501

Simultaneous estimation of aerosol optical constants and size distribution from angular light-scattering measurement signals*

Zhen-Zong He(贺振宗), Dong Liang(梁栋), Jun-Kui Mao(毛军逵)†, and Xing-Si Han(韩省思)

Jiangsu Province Key Laboratory of Aerospace Power System, College of Energy and Power Engineering, Nanjing University of Aeronautics and Astronautics, Nanjing 210016, *China*

(Received 26 December 2017; revised manuscript received 15 January 2018; published online 26 April 2018)

The angular light-scattering measurement (ALSM) method combined with an improved artificial bee colony algorithm is introduced to determine aerosol optical constants and aerosol size distribution (ASD) simultaneously. Meanwhile, an optimized selection principle of the ALSM signals based on the sensitivity analysis and principle component analysis (PCA) is proposed to improve the accuracy of the retrieval results. The sensitivity analysis of the ALSM signals to the optical constants or characteristic parameters in the ASD is studied first to find the optimized selection region of measurement angles. Then, the PCA is adopted to select the optimized measurement angles within the optimized selection region obtained by sensitivity analysis. The investigation reveals that, compared with random selection measurement angles, the optimized selection measurement angles can provide more useful measurement information to ensure the retrieval accuracy. Finally, the aerosol optical constants and the ASDs are reconstructed simultaneously. The results show that the retrieval accuracy of refractive indices is better than that of absorption indices, while the characteristic parameters in ASDs have similar retrieval accuracy. Moreover, the retrieval accuracy in studying L-N distribution is a little better than that in studying Gamma distribution for the difference of corresponding correlation coefficient matrixes of the ALSM signals. All the results confirm that the proposed technique is an effective and reliable technique in estimating the aerosol optical constants and ASD simultaneously.

Keywords: angular light-scattering measurement method, aerosol optical constants, aerosol size distribution, inverse radiation problem

PACS: 91.67.gp, 65.80.–g, 92.60.Mt, 43.20.Ye **DOI:** 10.1088/1674-1056/27/5/059101

1. Introduction

Aerosols play a crucial role in atmospheric radiative transfer by absorbing and scattering solar radiation, which results in climate degeneration, the greenhouse effect, etc. So, obtaining accurate and reliable data of the aerosol absorption and scattering properties is a prerequisite for studying the atmospheric radiative energy balance effectively.[1–5] Aerosol absorption and scattering properties depend on aerosol optical constants, aerosol size distribution (ASD), and morphology. Generally, the aerosol optical constant, a function of the chemical, phase composition and their mixing state, describes the optical properties and the interaction of the aerosol with radiation, while the ASD affects the meteorological phenomena and climatic trends.[6–10]

Generally, the aerosol optical constants and ASD cannot be obtained directly and often need to be retrieved with the help of some experimental data and corresponding inverse theories. Recently, coupled with some intelligent optimization algorithms, the optical measurement method, e.g., spectral extinction measurement, angular scattering measurement, optical depth measurement, or any combination of these, is regarded as a fast, nonintrusive, and convenient method to retrieve the ASD and aerosol optical constants.[5,11–18] However, accurate prediction of the optical constants and ASDs simultaneously is still regarded as a very challenging problem and needs further research.

In the present paper, the angular light-scattering measurement (ALSM) method, which has satisfactory performance in studying particle size distribution,[15,19,20] is proposed to estimate the aerosol optical constant and the ASD simultaneously. The inverse problem is solved by using an improved artificial bee colony (IABC) algorithm, which has been successful in solving the problem of retrieving the aerosol optical constants in our previous work.[11] Moreover, an optimized selection principle of measurement angles on the basis of the sensitivity analysis and principle component analysis (PCA) is proposed to improve the retrieval accuracy. The remainder of this paper is organized as follows. First, the principles of the ALSM method and the optimized selection principle of measurement angles are introduced. Then, the aerosol optical constants available on the AERONET and two common ASDs are estimated simultaneously under different random measurement errors. Finally, the main conclusions and prospects for further research are provided.

*Project supported by the Jiangsu Provincial Natural Science Foundation, China (Grant Nos. BK20170800 and BK20160794) and the National Natural Science Foundation of China (Grant No. 51606095).

†Corresponding author. E-mail: mjkpe@nuaa.edu.cn

© 2018 Chinese Physical Society and IOP Publishing Ltd

2. Direct problem

2.1. The angular light-scattering measurement (ALSM) method

According to the principle of the ALSM method, when a non-polarized parallel incident light beam with intensity I_0 impinges on a suspension particle system with the optical constants which are different from that of the medium (see Fig. 1), if the radiative transfer process satisfies the following conditions: 1) the particles distribute uniformly with random orientation, 2) the optical thickness of the sample is thin and the independent scattering of particles dominates, 3) the scattering phase function of the particle is symmetrical about the azimuthal angle and only a function of the polar angles, the light-scattering intensity at the angle θ can be expressed as follows:[15,19,21]

$$I(\theta) = \frac{\pi N_{\mathrm{D}}}{\lambda} \int_{D_{\min}}^{D_{\max}} i(\theta, m_\lambda, D, \lambda) f(D) \mathrm{d}D, \tag{1}$$

where $I(\theta)$ denotes the angular light-scattering intensity at measurement angle θ, which can be measured by a nephelometer; N_{D} is the total number concentration; $f(D)$ and m_λ denote the unknown ASD and the unknown aerosol optical constants at wavelength λ, respectively, which need to be determined; D denotes the diameter of the aerosol particle; $D_{\max}$ and $D_{\min}$ are the upper and lower integration limits, respectively; $i(\theta, m_\lambda, D, \lambda)$ denotes the light-scattering intensity of the aerosol particle with diameter D at measurement angle θ from the incident direction, which can be derived in terms of the Mie scattering functions $i_1(\theta, m_\lambda, D, \lambda)$ and $i_2(\theta, m_\lambda, D, \lambda)$ as[15,22,23]

$$i(\theta, m_\lambda, D, \lambda) = \frac{i_1(\theta, m_\lambda, D, \lambda) + i_2(\theta, m_\lambda, D, \lambda)}{8\pi^2} \lambda^2 I_0, \tag{2}$$

where I_0 denotes the incident measurement laser intensity.

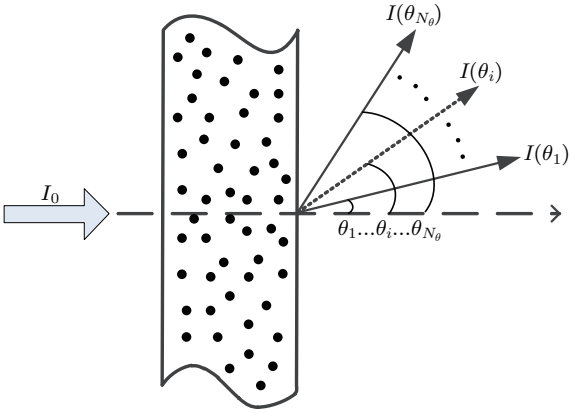


Fig. 1. Schematic model of the ALSM method.

In the present work, two common ASDs, i.e., the log-normal (L-N) and Gamma distributions, are studied. The mathematical representations of their volume frequency distributions are as follows:[24]

$$f_{\mathrm{L-N}}(D) = \frac{1}{\sqrt{2\pi} D \ln \sigma} \exp\left[-\frac{(\ln D - \ln \bar{D})^2}{2(\ln \sigma)^2} \right], \tag{3}$$

$$f_{\mathrm{Gamma}}(D) = D^\alpha \exp(-\beta D^\gamma), \tag{4}$$

where $\bar{D}$ and σ are the characteristic diameter and narrowness index in the L-N distribution function, respectively; α, β, and γ are the characteristic parameters in the Gamma distribution. Usually, in the modified form, $\gamma = 1$, so only parameters α and β in the Gamma distribution need to be investigated.[25] The particle size range is set from 0.001 μm to 10.0 μm in this study, which is the optimal measurement range in the optical measurement method.[26] The true values of the characteristic parameters in ASDs studied here are listed in Table 1. The optical constants of aerosol in this study obtained from the AERONET are depicted in Fig. 2.

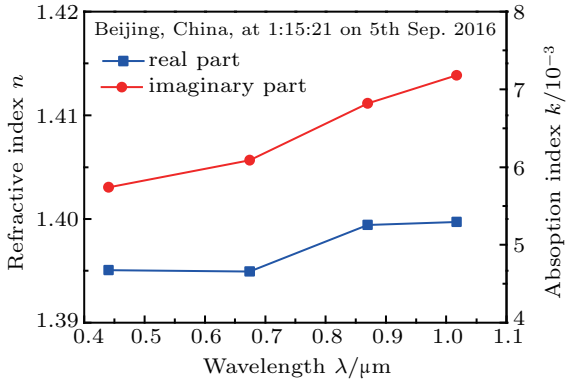


Fig. 2. (color online) Aerosol optical constants available on AERONET.[27]

Table 1. True values of characteristic parameters in the ASDs.

ASD functions	Parameters	True values
L-N	$(\bar{D}, \sigma)$	(0.6, 2.5)
Gamma	(α, β)	(6.0, 1.5)

2.2. An optimized selection principle of ALSM signals

Since the ALSM signals contain some important information about the particle system, it is necessary to gain insight into the influence of the ALSM signals on the retrieval accuracy in simultaneous retrieval of the aerosol optical constants and ASDs. Usually, different measurement angles obtain different measurement signals, which will lead to different retrieval accuracy. So, selecting optimal measurement angles is very important. In the present study, the sensitivity analysis of the ALSM signals to the optical constants or characteristic parameters in the ASDs at different measurement angles is employed to find the optimized selection region of measurement angles. Then, the contribution rate of the ALSM signals based on the PCA approach is studied to select the optimal measurement angles within the optimized selection region obtained by

the sensitivity analysis approach to improve the retrieval accuracy.

Usually, sensitivity analysis studies how the uncertainty in the output of a mathematical model or system (numerical or otherwise) can be apportioned to different sources of uncertainty in its inputs. The sensitivity coefficient, which is the first derivative of the ALSM signals $I(\theta)$ to the optical constants or characteristic parameters in the ASDs at a certain measurement angle θ, is proposed to carry out the sensitivity analysis of the ALSM signals. The sensitivity coefficient $\chi_a(\theta)$ is defined as[12,28]

$$\chi_a(\theta) = \frac{\partial I(a,\theta)}{\partial a} = \frac{I(a+\Delta a,\theta) - I(a-\Delta a,\theta)}{2\Delta a}, \quad (5)$$

where Δ represents a tiny change and is set 0.5% in this study; and a denotes the independent variable which stands for the optical constants or characteristic parameters in ASDs, $a = n$, k, $\bar{D}$, or σ. According to the definition of the sensitivity coefficient, it is obvious that the optimal measurement angles are in the region with larger absolute value of sensitivity coefficient generally. Figure 3 depicts the sensitivity coefficients of the ALSM signals to the optical constants or characteristic parameters in the L-N distribution. It is obvious that for the characteristic parameters in the L-N distribution and the optical constants, the sensitivity coefficients at forward scattering angles and backward scattering angles, i.e. $\theta < 40^\circ$ or $140^\circ < \theta$, are satisfactory as a whole. So, to ensure the retrieval accuracy in studying the L-N distribution, the optimal measurement angles are selected within $[0^\circ, 40^\circ] \cup [140^\circ, 180^\circ]$. Similar conclusion can be obtained in studying the Gamma distribution, and the corresponding optimal measurement angles are selected within $[0^\circ, 60^\circ] \cup [160^\circ, 180^\circ]$. The sensitivity analysis for the Gamma distribution is not shown here and interested readers can contact us for the details.

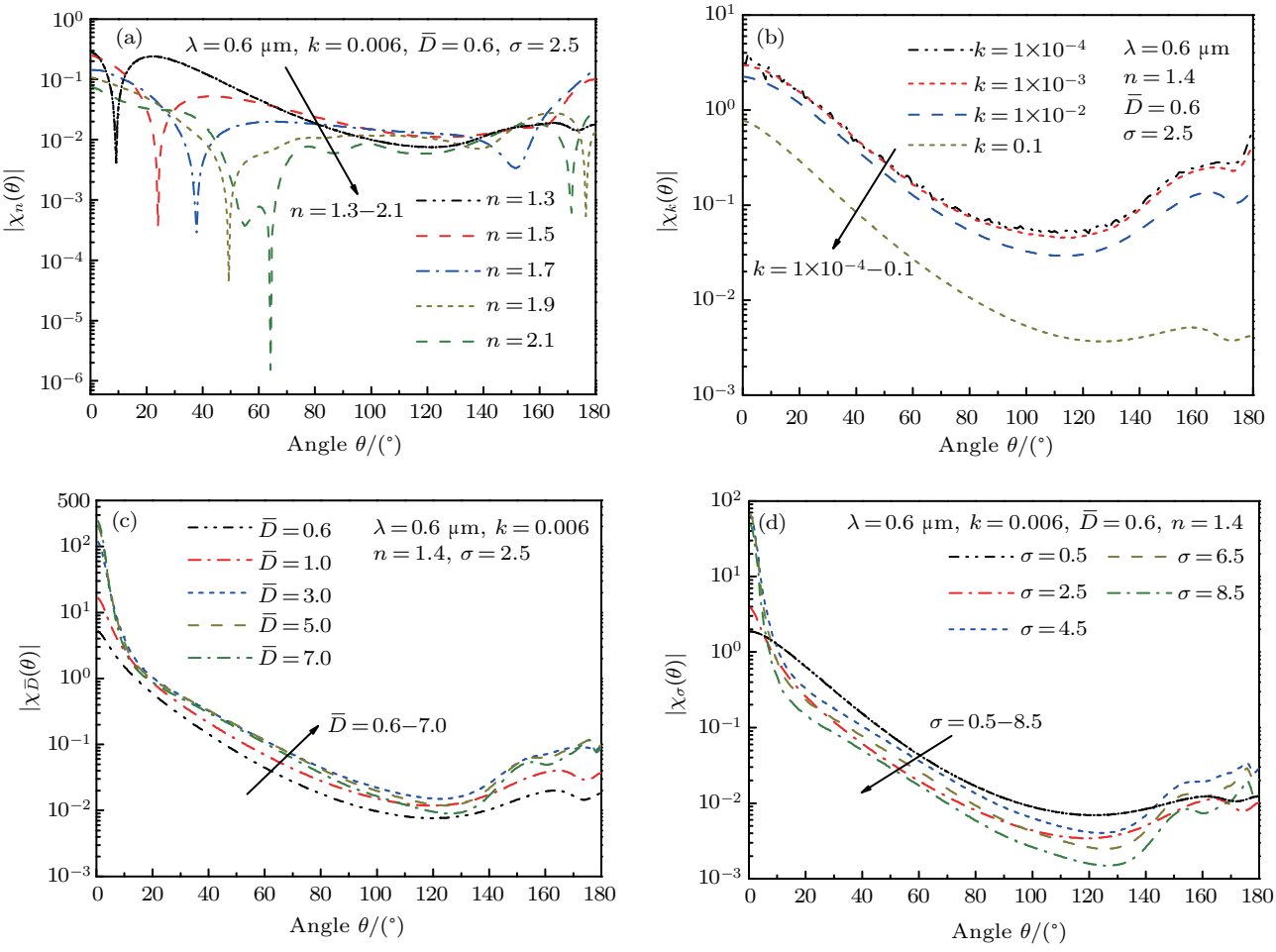


Fig. 3. (color online) Sensitivity coefficients of ALSM signals to optical constants or characteristic parameters in L-N distribution at different measurement angles.

The PCA approach is a feature extraction method commonly used in pattern recognition. Its basic idea is to convert a set of observations of possibly correlated variables into a new set of values of linearly uncorrelated variables called principal components, each of which is a linear combination of the original variables. Each of the principal components contains different amount of information, which can be measured by their contribution rate. Therefore, the original variables can be replaced by several principal components with highest contribution rates, achieving the purpose of dimen-

sion reduction.[29] Moreover, the contribution rate of the original variables to these principal components can be calculated by using a formula suggested by Chiang *et al.*[30] The PCA approach was used by Tang to study the optimized selection method of measurement wavelengths to improve the retrieval accuracy of particle size distribution.[31]

To provide the optimized selection measurement angles and improve the accuracy in simultaneous retrieval of the aerosol optical constants and ASDs, the PCA approach is proposed to study the contribution rate of the ALSM signals at different measurement angles within the optimized selection region obtained by the sensitivity analysis. According to the PCA approach, various possible combinations of the optical constants and characteristic parameters are considered and form an ALSM signals matrix. In the present study, the measurement angles in studying the L-N distribution vary from $[0°,40°]\cup[140°,180°]$ in steps of 5° (18 degrees), and those in studying the Gamma distribution vary from $[0°,60°]\cup[160°,180°]$ in steps of 5° (18 degrees). The refractive indices n vary from 1.3 to 2.1 in steps of 0.05 (17 values), and the imaginary indices k vary from 0.00001 to 0.5 in steps of 0.05 (11 values), which means that there will be about $17\times11=187$ combinations of the optical constants. The characteristic parameters in the ASDs, e.g., $\bar{D}$ and σ, are assumed to vary from 0.1 to 10.1 in steps of 0.5 (21 values), which means that there will be about $21\times21=441$ combinations of the characteristic parameters in the ASDs. As the optical constants and characteristic parameters in the ASDs are independent from each other, there are about $187\times441=82467$ combinations of n, k, $\bar{D}$, and σ. So, a 18×82467 ALSM signals matrix I for the L-N distribution and Gamma distribution can be constructed as follows:

$$\boldsymbol{I}=\begin{bmatrix} I(\theta_1)_1 & & \cdots & & I(\theta_S)_1 \\ I(\theta_1)_2 & \cdots & I(\theta_i)_{j-1} & \cdots & \\ \vdots & I(\theta_{i-1})_j & I(\theta_i)_j & I(\theta_{i+1})_j & \vdots \\ & & \vdots & I(\theta_i)_{j+1} & \vdots \\ I(\theta_1)_{82467} & & \cdots & & I(\theta_S)_{82467} \end{bmatrix}, \quad (6)$$

where S denotes the number of measurement angles, $S=18$. In matrix $\boldsymbol{I}$, each column is an observation at a particular angle θ_i, and each row represents a kind of combination of optical constants and characteristic parameters in the ASDs. To highlight the difference among the contributions of the components, the Savitzky–Golay smoothing is applied to each column of matrix $\boldsymbol{I}$. According to matrix $\boldsymbol{I}$, the correlation coefficient matrix $\boldsymbol{R}$ between the column vectors can be obtained as follows:[32]

$$\boldsymbol{R}=(R_{ij})=\mathrm{corrcoef}(\boldsymbol{I}),\quad i,j=1,2,\ldots,S, \quad (7)$$

where R_{ij} denotes the correlation coefficients between the column vectors $I(\theta_i)$ and $I(\theta_j)$; corrcoef is a function for calculating the correlation coefficient matrix. Figure 4 depicts the correlation coefficient matrix of ALSM signals matrix $\boldsymbol{I}$, and the color in each cell indicates the magnitude of the correlation coefficient. The blue color denotes a perfect correlation and red denotes no correlation. The range of R_{ij} is [0, 1] with 1 being a perfect correlation and 0 being no correlation. The diagonal line indicates the highest correlation 1, which is represented in blue. The redder the tone is, the lower the absolute value of the correlation will be. The correlation matrix is always symmetrical with the values in the lower left always being a mirror of the values in the upper right. The red color box expresses the low correlation between the adjacent two extinction column vectors, which demonstrates little information redundancy at the two extinction data.

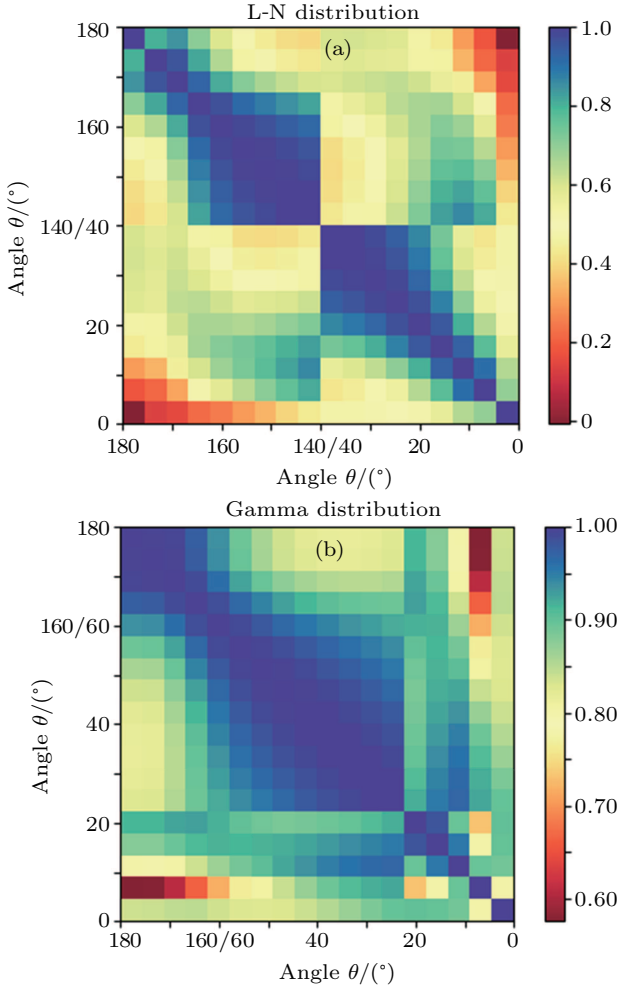


Fig. 4. (color online) Correlation coefficient matrix of the ALSM signals for different combinations of the optical constants and characteristic parameters in different ASDs: (a) L-N distribution, (b) Gamma distribution.

The eigenvectors and eigenvalues for the correlation coefficient matrix $\boldsymbol{R}$ are derived as.[32]

$$\boldsymbol{R}\gamma_i=\gamma_i\boldsymbol{v}_i,\quad i=1,\ldots,h, \quad (8)$$

where the eigenvalues attained by descending order are $\gamma_1\geq\gamma_2\geq\cdots\geq\gamma_h$, and the corresponding eigenvector matrix is $\boldsymbol{V}=[\boldsymbol{v}_1,\ \boldsymbol{v}_2,\ \ldots,\ \boldsymbol{v}_h]$, h is the dimension of matrix $\boldsymbol{R}$. Then,

the accumulated contribution ratio of the former z principal components can be obtained as[32]

$$V_z = \sum_{i=1}^{z} \gamma_i / \sum_{i=1}^{h} \gamma_i. \tag{9}$$

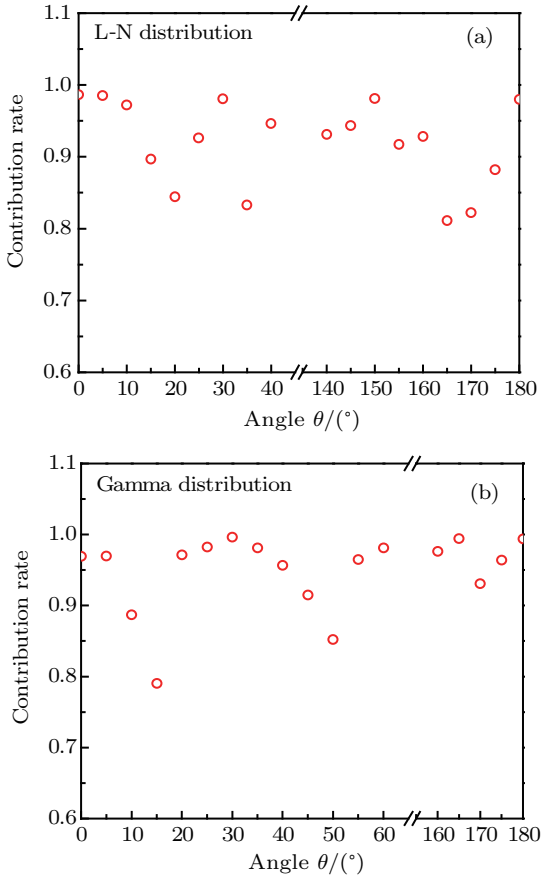


Fig. 5. (color online) Contribution rates of the ALSM signals to the principle components for different ASDs: (a) L-N distribution, (b) Gamma distribution.

According to Tang's work,[31] z is determined by letting V_z not less than 90%, which denotes that the original data can be represented well with the new z principal components. Therefore, the contribution rate of the ALSM signals at measurement angle θ_i to the overall z principal components is expressed as[32]

$$y_i = \sum_{j=1}^{z} \gamma_k v_{ik}^2 / \omega_{ii}, \tag{10}$$

where ω_{ii} denotes the value in the principal diagonal of $\boldsymbol{R}$. For different ASDs, the values of z are 5 (L-N distribution) and 3 (Gamma distribution), and the contribution rates of the ALSM signals at different measurement angles to the principle components for different ASDs are depicted in Fig. 5. According to the PCA approach, the ALSM signal with larger contribution rate will be given priority to retrieve PSDs, and the corresponding wavelength will be selected more likely as the optimal measurement wavelength. For the L-N distribution, the former 7 angles with the highest contribution rate are θ=0°, 5°, 150°, 30°, 180°, 10°, 40°; for the Gamma distribution, the former 7 angles with the highest contribution rate are $\theta = 30°, 165°, 180°, 115°, 25°, 35°, 60°$. The measurement angles used in the following study are selected according the optimized selection principle mentioned above.

2.3. The inverse problem model

The improved artificial bee colony algorithm is proposed as the inverse problem method, which has been used to study the optical constants successfully. The detail procedure of the IABC is not available in this paper and can be found in our previous work.[11]

For simultaneous estimation of the aerosol optical constants and ASD, there are four parameters to be determined, i.e., the refractive and absorption indices of optical constants (n and k) and the characteristic parameters in the ASDs ($\bar{D}$ and σ or α and β). Usually, increasing the number of measurement angles N_θ and the scale of swarm size SN will increase the retrieval accuracy as well as the cost of calculation and experiment. So, to improve the retrieval accuracy while reducing costs, the number of measurement angles and the scale of swarm size should be studied first.

Usually, the inverse problem is solved by minimizing the objective function F_{obj}, which is defined as the sum of the square residual between the simulated and the measured signal ratios. The mathematical expression of F_{obj} is derived as follows:

$$F_{\text{obj}} = \sqrt{\frac{1}{N_\theta} \sum_{i=1}^{N_\theta} \left(\frac{I(\theta_i)_{\text{sim}} - I(\theta_i)_{\text{mea}}}{I(\theta_i)_{\text{mea}}} \right)^2}, \tag{11}$$

where N_θ denotes the number of measurement angles; and $I(\theta_i)_{\text{sim}}$ and $I(\theta_i)_{\text{mea}}$ denote the simulated and the measured ALSM signals, respectively. Figures 6 and 7 compare the objective functions under different scales of swarm size and different numbers of measurement angles selected according to the optimized selection principle in solving the problem of simultaneous retrieval of the aerosol optical constants for the L-N distribution at wavelength $\lambda = 0.869$ μm ($m = 1.399 + 0.00682$i). The system control parameters of the IABC are listed in Table 2. The termination criteria are set as: 1) the iteration accuracy is 10^{-16} and 2) the maximum iteration times are 3000. From Figs. 6 and 7, it can be found that the retrieval accuracy will be improved with increasing N_θ and SN, while the convergence speed is not the case. The satisfactory retrieval accuracy and convergence speed can be obtained with $SN = 40$ and $N_\theta = 5$. A similar conclusion can be drawn in studying the Gamma distribution. Therefore, the number of measurement angles is set as 5 (i.e., $\theta = 0°$, 5°, 150°, 30°, 180° for the L-N distribution and $\theta = 30°$, 165°, 180°, 115°, 25° for the Gamma distribution), and the scale of swarm size is set as 40 in this study.

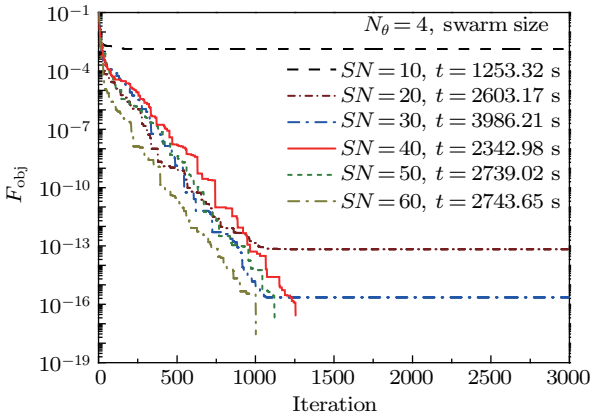


Fig. 6. (color online) Comparison of objective function values under different scales of swarm size.

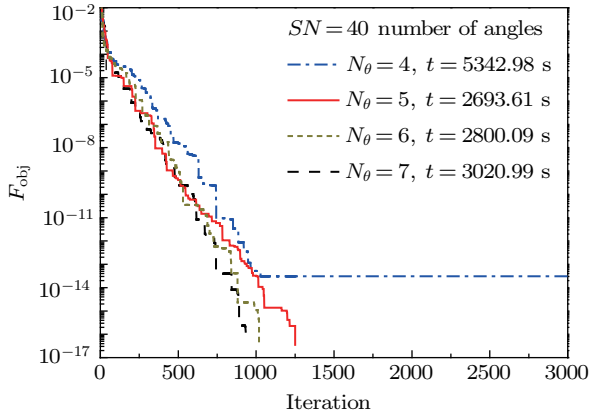


Fig. 7. (color online) Comparison of objective function values under different numbers of measurement angles.

Table 2. System control parameters of the IABC algorithm.

Parameter	N_θ	M	ε_0	limit	μ	F	C_R
IABC	4	3000	10^{-16}	100	4.0	0.5	0.4

3. Numerical simulation

Considering that the inverse algorithm is a stochastic optimization method and the optimization process has certain randomness, all the calculations are repeated 30 times. The numerical simulation procedure is illustrated in Fig. 8. The standard deviation of the inverse results of the optical constants η_X is investigated to evaluate the reliability and feasibility of the inverse results, and the mathematical expressions are described as follows:

$$\eta_X = \sqrt{\frac{1}{30}\sum_{i=1}^{30}(\bar{X}_{\text{sim}} - X_{\text{sim},i})^2},$$
$$\bar{X}_{\text{sim}} = \frac{1}{30}\sum_{i=1}^{30} X_{\text{sim},i}, \quad X = n \text{ or } k. \tag{12}$$

In addition, the relative deviation of the ASDs, δ, which means the sum of the deviation between the probability distribution estimated from the inverse calculation and the true ASDs in every subinterval, is studied to evaluate the estimated quality of the ASDs, and its mathematic expression is given as

$$\delta = \frac{\left\{\sum_{i=1}^{N}\left[f_{\text{est}}(\tilde{D}_i) - f_{\text{true}}(\tilde{D}_i)\right]^2\right\}^{1/2}}{\left\{\sum_{i=1}^{N}\left[f_{\text{true}}(\tilde{D}_i)\right]^2\right\}^{1/2}}, \tag{13}$$

where N denotes the number of subintervals which the particle size range $[D_{\min}, D_{\max}]$ is divided into; $\tilde{D}_i$ is the midpoint of the i-th subinterval $[D_i, D_{i+1}]$; $f_{\text{true}}(\tilde{D}_i)$ is the true ASD in the i-th subinterval; and $f_{\text{est}}(\tilde{D}_i)$ is the estimated ASD in the i-th subinterval.

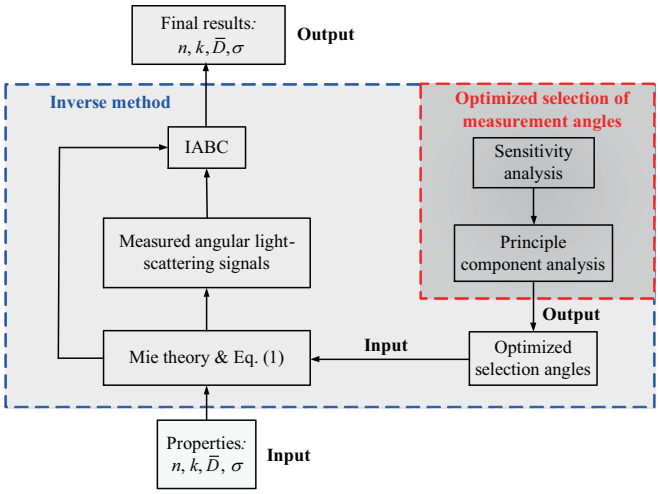


Fig. 8. (color online) Flowchart of the whole numerical simulation procedure.

To demonstrate that the optimized selection principle of measurement angles can improve the inverse accuracy effectively, we show in Table 3 the comparison of retrieval results in simultaneously retrieving the optical constants at $\lambda = 0.869$ μm ($m = 1.399 + 0.00682$i) and the characteristic parameters in the L-N distribution by using the optimized selection measurement angles and 15 groups of random selection measurement angles. In Table 3, the zero group denotes the optimized selection measurement angles, and the other ones denote the random selected angles. The retrieval results for the characteristic parameters in ASDs are also shown in Table 3, and those for the aerosol optical constants are depicted in Fig. 9. It is obvious that by using the optimized selection measurement angles, the relative deviation δ of the ASD is no more than 1%, and the retrieval accuracy for the optical constants is satisfactory. When the measurement angles are selected randomly, the deviations between the true values and the retrieval results are not controllable, and the largest relative error for the unsolved parameters reaches 16.86%, which means that the simultaneous retrieval accuracy of the optical constants and ASDs is uncontrollable. So, to ensure the retrieval accuracy, the optimized selection measurement angles are proposed.

Table 3. Retrieval results of different measurement angles selected according to different selection principles.

Number of solution	Measurement angles $\theta/(^\circ)$	Relative deviation δ	Number of solution	Measurement angles $\theta/(^\circ)$	Relative deviation δ
0	0, 5, 150, 30, 180	0.006104	8	134, 3, 65, 71, 94	0.143452
1	93, 95, 110, 133, 41	0.030237	9	153, 63, 91, 111, 78	0.007023
2	68, 107, 133, 127, 128	0.007569	10	170, 178, 105, 54, 88	0.002514
3	140, 124, 71, 176, 53	0.004792	11	151, 107, 122, 136, 144	0.027348
4	157, 168, 91, 63, 93	0.026655	12	178, 69, 51, 166, 102	0.149713
5	23, 72, 75, 165, 64	0.005843	13	79, 5, 112, 54, 36	0.222641
6	106, 162, 36, 143, 81	0.133768	14	158, 71, 167, 169, 73	0.015431
7	68, 37, 17, 73, 27	0.033487	15	174, 21, 109, 163, 17	0.024798

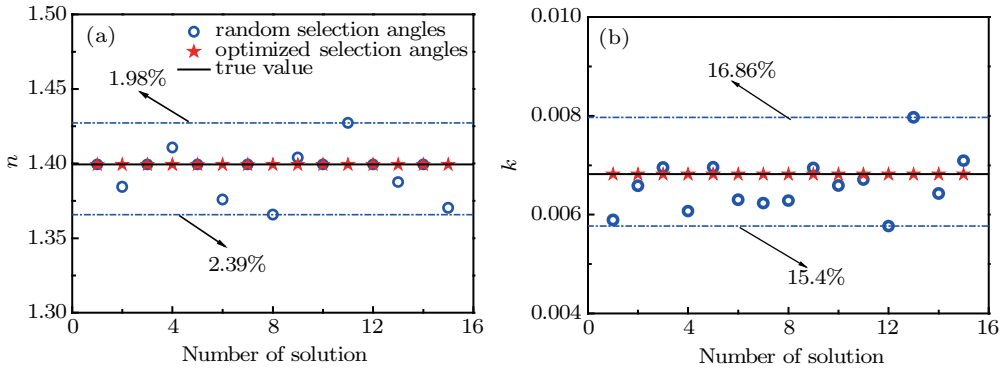


Fig. 9. (color online) Comparison of retrieval results by using the optimized selection measurement angles and those by using random selection measurement angles: (a) refractive index n, (b) absorption index k.

With the help of the IABC algorithm and the optimized selection principle of measurement angles, the optical constants and the ASDs mentioned above are reconstructed simultaneously. The searching ranges of the refractive and absorption indices are set as [1.3, 2.1] and [0.00001, 0.5], respectively, and the searching ranges of the characteristic parameters in ASDs are all set as [0.1, 10.1]. The average retrieval results of the optical constants are depicted in Figs. 10 and 11, and standard deviations and relative errors of the retrieval results are also shown in the figures. The retrieval curves of the ASDs are shown in Fig. 12. From Figs. 10 and 11, it is obvious that without random measurement error, the retrieval accuracy for the optical constants is most satisfactory, especially for the L-N distribution. The standard errors and relative errors will become larger when more random measurement errors are added to the measurement signals. Moreover, it can be found that the retrieval accuracy of the refractive index is better than those of absorption index under the same random measurement errors, which means that the monodromy characteristics of the estimated results of the refractive index are better than those of the absorption index. Figure 12 shows that the deviation between the true curves and the simulated ones becomes larger if the random measurement errors increase. Moreover, under the same measurement errors, the retrieval accuracy of ASD in studying the L-N distribution is little better than that in studying the Gamma distribution, which could attribute to the difference of the corresponding correlation coefficient matrixes of the ALSM signals (see Fig. 4). As a whole, the present methodology provides a very effective and promising technique to solve the problem of simultaneous retrieval of the aerosol optical constants and ASDs more accurately and reliably.

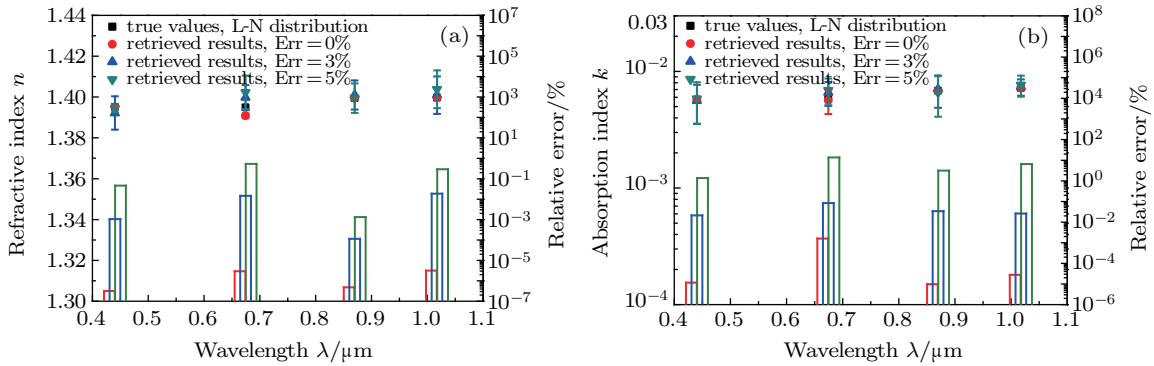


Fig. 10. (color online) Retrieval results of aerosol optical constants under different random measurement errors in studying L-N distribution: (a) refractive index n, (b) absorption index k.

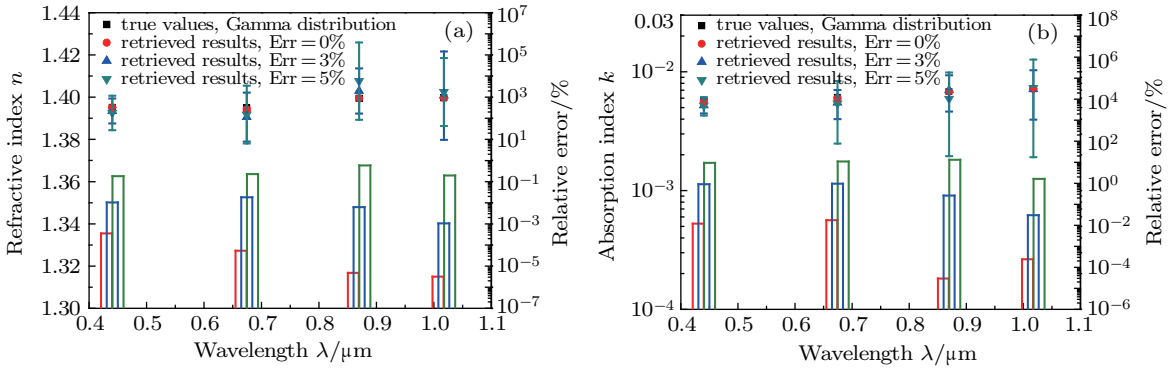


Fig. 11. (color online) Retrieval results of aerosol optical constants under different random measurement errors in studying Gamma distribution: (a) refractive index n, (b) absorption index k.

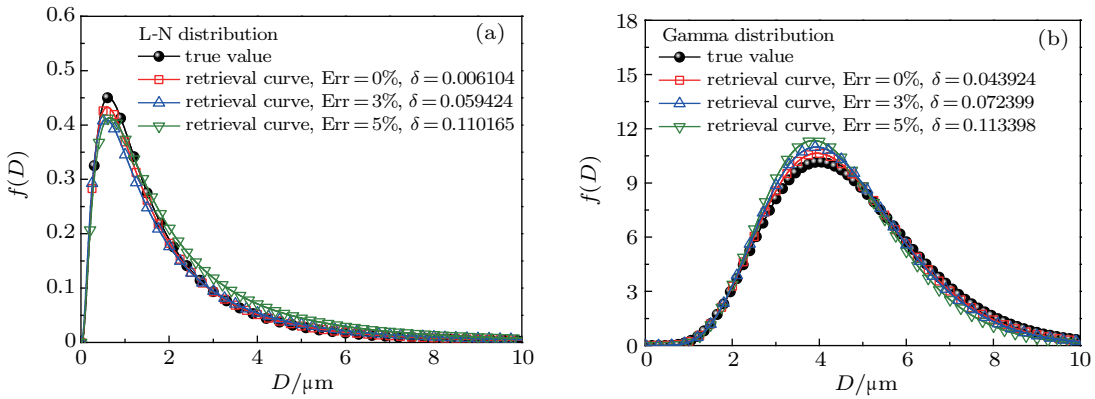


Fig. 12. (color online) Retrieval curves of different ASDs under different measurement random errors: (a) L-N distribution, (b) Gamma distribution.

Figure 13 shows the distributions of 30 retrieval results in retrieving the L-N distribution at $\lambda = 0.869$ μm under different random measurement errors. It can be found that the distributions of the estimated results disperse with increasing random measurement errors; the larger the random error is, the more dispersive the distribution will be. The relative error of $\bar{D}$ is similar to that of σ, while the largest relative error of absorption index is 137.24%, which is much larger than that of refractive index. A similar conclusion can also be obtained in studying the Gamma distribution, and the details are not shown for simplicity. All these phenomena also confirm the results obtained above.

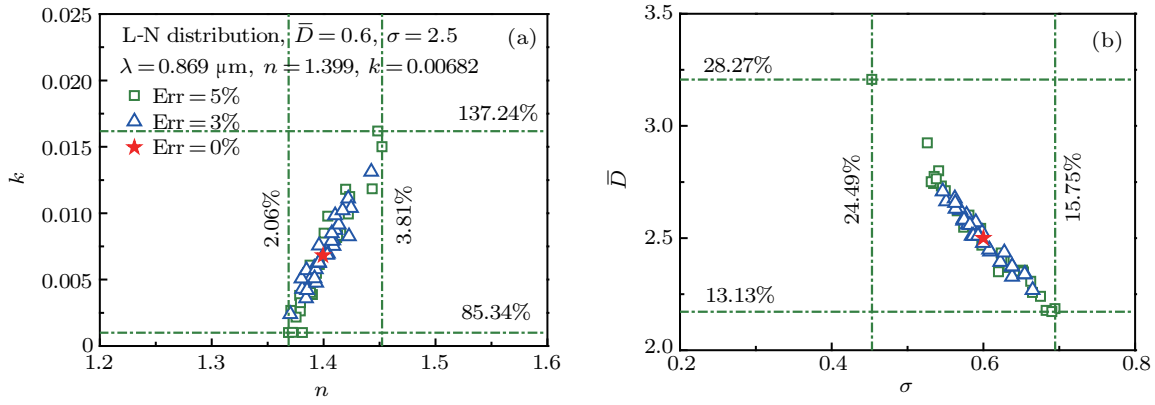


Fig. 13. (color online) Distribution of 30 retrieval results in retrieving the L-N distribution at $\lambda = 0.869$ μm under different measurement errors: (a) k, (b) $\bar{D}$.

4. Conclusions

Combined with an improved artificial bee colony algorithm, the angular light-scattering measurement method is applied to estimate optical constants and aerosol size distribution simultaneously. Moreover, to improve the retrieval accuracy, an optimized selection principle of the ALSM signals based on the sensitivity analysis and principle component analysis is proposed. The following conclusions can be drawn. (i) To simultaneously estimate the aerosol optical constants and size distribution accurately, the number of measurement an-

gles and the swarm scale in the IABC algorithm would be better set as 5 and 40, respectively. (ii) Comparing with random selection measurement angles, the optimized selection measurement angles can provide more useful information to ensure the accuracy of simultaneous estimation of the aerosol optical constants and size distribution. (iii) The retrieval accuracy of refractive indices of optical constants is better than that of absorption indices of optical constants, while the characteristic parameters in the ASDs have similar retrieval accuracy. (iv) The accuracy of the retrieval results in studying the L-N distribution is a little better than that in studying the Gamma distribution, which is attributed to the difference of the corresponding correlation coefficient matrixes of the ALSM signals.

Finally, as the aerosol particle is treated as a homogenic spherical particle in this study, the methodology presented here can also be used to study the simultaneous estimation of the optical constants and size distribution of other spherical particle dispersion medium, e.g., microalgae dispersion medium. Furthermore, as more measurement signals can be obtained by using the ALSM method, the methodology can also be proposed to simultaneously predict the optical constants and size distribution of non-spherical particles, which will be studied in our future work.

References

[1] Zhang Y C, Chen Y M, Fu X B and Luo C 2016 *Infrared Phys. Techn.* **77** 375

[2] Ebert M, Weinbruch S, Rausch A, Gorzawski G, Helas G and Hoffmann P 2002 *J. Geophys. Res-Atmos.* **107** 3

[3] Ebert M, Weinbruch S, Hoffmann P and Ortner H M 2004 *Atmos. Environ.* **38** 6531

[4] Sabatini, Roberto, Richardson and Mark 2013 *Infrared Phys. Techn.* **56** 30

[5] Liu Q, Huang H H, Wang R, Wang G S, Cao Z S, Liu K, Chen W D and Gao X M 2014 *Chin. Phys. B* **23** 064205

[6] Spindler C, Riziq A A and Rudich Y 2007 *Aerosol Sci. Tech.* **41** 1011

[7] Flores J M, Washenfelder R A, Adler G, Lee H J, Segev L and Laskin J 2014 *Phys. Chem. Chem. Phys.* **16** 10629

[8] Han X, Shen J, Yin P, Hu S and Bi D 2014 *Opt. Commun.* **316** 198

[9] Tammet H and Kulmala M 2014 *J. Aerosol Sci.* **77** 145

[10] Tao Z M, Zhang Y C, Liu X Q, Tan K, Shao S X, Hu H L, Zhang G X and Lv Y H 2004 *Chin. Phys. B* **13** 409

[11] He Z Z, Mao J K and Han X S 2017 *Optik* **145** 316

[12] Ren Y T, Qi H, Chen Q, Ruan L M and Tan H P 2015 *Opt. Express* **23** 19328

[13] Ruan L M, Wang X Y, Qi H and Wang S G 2011 *J. Aerosol Sci.* **42** 759

[14] Chen Q X, Yuan Y, Shuai Y and Tan H P 2016 *Atmos. Environ.* **135** 84

[15] Ye M, Wang S, Lu Y, Hu T, Zhu Z and Xu Y 1999 *Appl. Opt.* **38** 2677

[16] Zuo H Y and Yang J G 2007 *Acta Phys. Sin.* **56** 6132 (in Chinese)

[17] Ren Y T, Qi H, Yu X Y and Ruan L M 2017 *Opt. Commun.* **389** 258

[18] Si F Q, Liu J G, Xie P H, Zhang Y J, Liu W Q, Kuze H, Liu C and Lagrosas N 2005 *Chin. Phys. B* **14** 2360

[19] Wang Y, Liang G and Pan Z 2010 *Particuology* **8** 365

[20] Mroczka J and Szczuczyński D 2013 *J. Quant. Spectrosc. Ra.* **129** 48

[21] Vargas-Ubera J, Aguilar J F and Gale D M 2007 *Appl. Opt.* **46** 124

[22] Dombrovsky L A and Baillis D 2010 *Thermal Radiation in Disperse Systems: An Engineering Approach*, (New York: Begell House) pp. 135–244

[23] Modest M F 2013 *Radiative Heat Transfer* (3rd Edn.) (New York: McGraw-Hill) pp. 387–437

[24] Sun X G, Tang H and Dai J M 2009 *Powder Technol.* **190** 292

[25] He Z Z, Hong Q, Chen Q and Ruan L M 2016 *Particuology* **28** 6

[26] Yuan Y, Yi H L, Shuai Y, Wang F Q and Tan H P 2010 *J. Quant. Spectrosc. Ra.* **111** 2106

[27] Aerosol robotic network (AERONET). 2014. NASA <http://aeronet.gsfc.nasa.gov/>

[28] Kamrunnahar M, Braatz R D and Alkire R C 2004 *J. Electrochem. Soc.* **151** 90

[29] Jolliffe I 2002 *Principal Component Analysis* (Wiley Online Library) pp. 513–520

[30] Chiang L H and Pell RJ 2004 *J. Process Contr.* **14** 143

[31] Tang H and Lin J Z 2013 *J. Quant. Spectrosc. Ra.* **115** 78

[32] He Z Z, Mao J K and Han X S 2018 *Powder Technol.* **325** 510